



Mechanism and visualization of streamline adjustment in enhanced oil recovery: a comparative study between well pattern adjustment and polymer flooding

Yu Li¹ · Huiqing Liu¹ · Xiaohu Dong¹ · Qing Wang² · Wuchao Wang² · Zhipeng Wang²

Received: 31 May 2022 / Accepted: 15 April 2023 / Published online: 31 May 2023
© The Author(s) 2023

Abstract

Due to the long-term scouring of steam/water flooding, the water channels restricts the expansion of streamlines in the swept region. The formation of the main streamline, an inevitable and troublesome challenge during steam/water flooding, restrict the spread of the sweep region and the oil extraction in oil reservoirs. To realize the swept main streamlines adjustment (SA), well pattern adjustment (WPA) and polymer flooding (PF) are the mature technologies applied in the development of reservoir. The WAF and PF, as two kinds of oil extracting methods with different principles and operations, is difficult to directly verify the disturbance law to main streamlines in the same model or experimental physical field. Two-dimensional sand-packed model can elucidate the mechanism of WPA and PF for SA based on the direct processing of images and data analysis of production data. Through the oil–water distribution images from displacement experiment, the influence of viscous fingering generated by streamlines development can be obtained and described by the mathematical model to illustrate the relationship between penetration intensity and mobility ratio. In addition, the dynamic production data can reflect the change of flow resistance and water cut during the expansion of swept region. Based on observations of macro and micro perspectives, the experimental results show that the WPA greatly expands the coverage region of the streamlines, while PF makes the streamlines denser in the swept region. By comparing the distribution of streamlines between the two methods, the different shapes of streamlines are deeply influenced by the mobility ratio that determines the viscous fingering and the well pattern type. Finally, the adaptability of different methods for extracting the remaining oil is proposed. The WPA pays attention to improving the macro sweep efficiency outside the swept region. Meanwhile, the PF strategy pays more attention to improving the micro sweep efficiency in the swept region. The analysis of single-factor shows that viscous fingering has an obvious interference effect on the streamline morphology development, which highlights the meaning and importance of using the synergistic effect of WPA and PF to enhance oil recovery.

Keywords Visual sand-packed model · Streamline adjustment · Well pattern adjustment · Polymer flooding · Macroscopic and microscopic analysis

List of symbols

A The cross-sectional area of model, cm^2
 A_s Area of swept region, cm^2
 C_p Potential-distance ratio coefficient, s^{-1}
 K_{in} Permeability of displacing region, μm^2

M_{in} Mobility ratio
PF Polymer flooding
PWF Primary water flooding
SWF Subsequent water flooding
 g Gravitational acceleration, $\text{Kg}/(\text{m}^2 \text{ s})$
 p Pressure of the fluid, Pa
 r_{inj} The radius of the injection well, cm
 u_{in} Percolation velocity of displacing fluid, cm/s
 v_{oi} Original oil volume, mL
 ε Viscous fingering distance, cm
 μ_i Viscosity of the fluid in porous media, Pa s
 σ Change rate of viscous fingering
 ϕ The porosity
 A_o Area of the region with oil, cm^2

✉ Huiqing Liu
ly15872410897@163.com

¹ State Key Laboratory of Petroleum Resources and Prospecting, China University of Petroleum, Beijing 102249, China

² MOE Key Laboratory of Petroleum Engineering, China University of petroleum, Beijing 102249, China

C	The constant of the potential, $\mu\text{m}^2 \text{s}^{-1}$
DPR	Disproportionate permeability reduction
K_{ed}	Permeability of displaced region, μm^2
OOIP	Original oil-in-place
PV	Pore volume injection, cm^3
SNA	Reservoir abundance of oil, cm
VF	Viscous fingering
n	Distance in the normal direction, cm
r_f	The radius of the displacement front, cm
r_{pro}	The radius of the production well, cm
v_i	Velocity of the liquid, cm^3/s
α	Horizontal angle of the model
λ	The mobility of fluid
ρ_i	Density of the fluid, Kg/m^3
τ	The time, s
Φ_r	Velocity potential, $\mu\text{m}^2/\text{s}$

Introduction

As global energy demand increases, more crude oil needs to be extracted from existing fields. However, only approximately 30% of the original oil in place (OOIP) can be extracted from oil fields (Cheraghian 2015). Currently, tertiary oil recovery techniques and well pattern adjustment (WPA) methods have already been adopted to develop the remaining oil efficiently (Pei et al. 2012). After the long-term water scouring, the heterogeneity of the reservoir is aggravated, which greatly restricts the development performance of oil reservoirs (Imqam et al. 2017). On one hand, due to the high flow ability of the water channels, primary water flooding (PWF) has a poor development performance on the remaining oil after primary recovery. On the other hand, it also causes environmental issues in the process of disposing of large amounts of produced water (Wei et al. 2014; Zheng et al. 2021).

Some experts have proposed polymer flooding (PF) to adjust the mobility profiles in the reservoir (Jian et al. 2008; Liu et al. 2020). The PF realizes SA to improve oil recovery by increasing the viscosity of the flooding fluid. In addition, the viscoelasticity of polymer can improve the oil washing efficiency (Sandiford 1964; Wang et al. 2000; Wu et al. 2016; Zolfaghari et al. 2018; Du et al. 2019). Other experts have proposed WPA can effectively improve oil recovery by either infusing or adding new streamlines (Yuan and Yang 2003; Van and Chon 2016; Zhiwang et al. 2018; Wang et al. 202a). After primary water flooding, the water channels along the injection-production well line have a higher-pressure conductivity, resulting in no displacing fluid (water) reaching the unswept region. To overcome this challenge, WPA and PF can achieve effective and flexible performance in reservoirs, reflecting in the complex changes of the streamline. The experimental studies show that WPA and PF can

change the direction of pressure conduction in the reservoir (Grinestaff 1999; Samier et al. 2001; Shams et al. 2003; Zhao et al. 2020). In addition to polymer flooding, there are many more chemical flooding techniques applied in streamlines adjustment, such as foam flooding, water-altering-gas process (WAG), chemically enhanced water alternating gas (CWAG), alkali-surfactant-polymer (ASP) flooding, colloidal dispersion gel flooding and nanomaterials flooding (Mack and Smith 1994; Christensen et al. 2001; Behzadi and Towler 2009; Wang et al. 2010; Tongwa and Bai 2016; Guo and Aryana 2018). However, due to the complex chemical composition of the technology, the mechanism is very complicated and involves many influencing factors.

Whether using numerical simulation method or experimental method, it is challenging to describe the swept region intuitively. The streamline description can vividly describe the flow characteristics in the porous media (Samier et al. 2001). And the two-dimensional sand-packed model can directly reflect the change of streamline and the distribution of the remaining oil (Cottin et al. 2010; Al-Shalabi and Ghosh 2016; Jackson et al. 2017; Wang et al. 2020). Some experts studied the heterogeneous phase combination flooding for oil recovery enhancement by using the 2D sand-packed model. The characteristics of the remaining oil under different SA measures were identified through micro-model images. Furthermore, identifying and validating the oil recovery mechanisms through qualitative and quantitative analyses of static and dynamic displacement is critical (Pratama and Babadagli 2021).

In the paper, visual experiments are used to study the influence of different methods on streamlines:

1. Explore the influence of WPA strategy on streamline distribution. Explain the mechanism of WPA based on SA to enhance oil recovery.
2. Explore the influence of PF strategy on streamline fraction to reflect the mechanism of enhanced oil recovery on macro and micro scales.
3. Through the comparison of the two SA methods, study whether there are significant differences in the shape of streamline distribution.

Experimental methods

Experimental materials

The visual sand-packed model is designed to study the distribution of streamlines. The visual experiment model consists of two iron plates 15 mm thick, with eight penetrating holes as shown in Fig. 1a. And the model also has two glass plates 20 mm thick, possessing the same penetrating holes as the iron plates. The heat-resistant colloid is laid inside

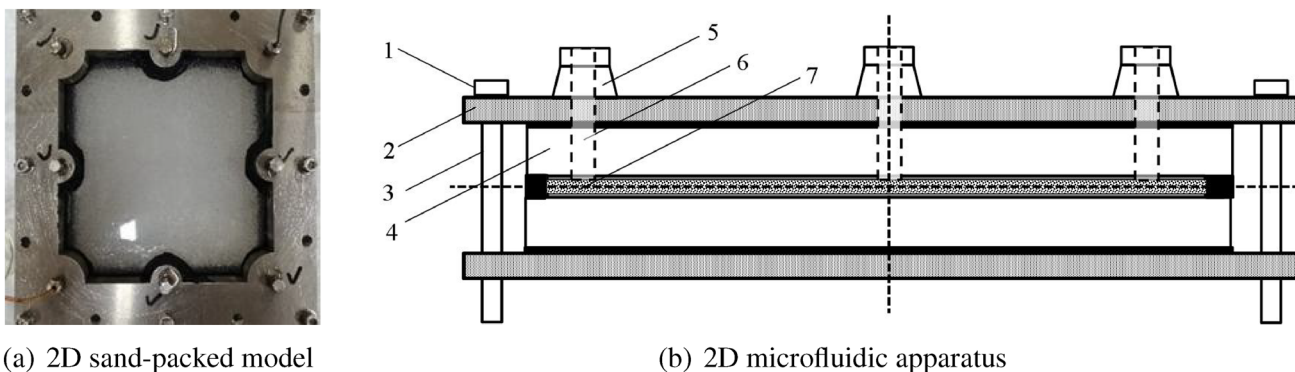


Fig. 1 The images of 2D experimental apparatus. 1-nut; 2-iron plate; 3-bolt; 4-glass plate; 5-joint; 6-penetrating hole; 7-glass beads layer

two glass plates to fix the glass beads (380 μm) which simulate the rock skeleton. The glass beads are filled into a gap between two glass plates to form the simulated reservoir (Wu et al. 2016). The thickness of the simulated reservoir is determined by the mesh size of the glass beads. All sides of the simulated reservoir are sealed around with heat-resistant and stretch-resistance glass glue, which ensures the tightness of the model. The visual sand-packed model is featured with great transmittance, which allows us to directly observe the movement and distribution of fluid in the simulated reservoir (Lu et al. 2017).

The glass beads with good chemical stability, are produced by Dongguan Jinying Abrasive Technology Co., Ltd, which. These glass plates are produced by Shenyang Huamei Quartz Co., Ltd, which could resist the pressure of 3 MPa. The size of the glass plate is 250 mm × 250 mm × 20 mm. These iron plates are produced by Jiangsu Lianyou Scientific Research Instrument Co., Ltd. After assembly and

airtightness treatment, the visual sand-packed model is built to simulate multiple well patterns as shown in Fig. 1b.

The size of the visual region is 200 mm × 200 mm. The thickness of the simulated reservoir depends on the properties and compressibility of the glass beads and heat-resistant colloid, which makes it difficult to measure reservoir thickness. However, because fluid percolation distance in the vertical direction is far less than that in the horizontal, there is no need to measure the thickness of the reservoir in the visual sand pack model. In the work, the size of glass beads is 40 mesh, resulting in the simulated reservoir thickness of about 800 μm. The pore volume reached 56.7 mL through the saturated water process, and the porosity reached about 0.177. The initial water saturation reached about 14%.

Establishing the appropriate experimental system to realize the various types of well pattern designed in the experimental scenarios. The visual sand-packed model was connected to the displacement power system and the dynamic monitoring system as shown in Fig. 2. The displacement

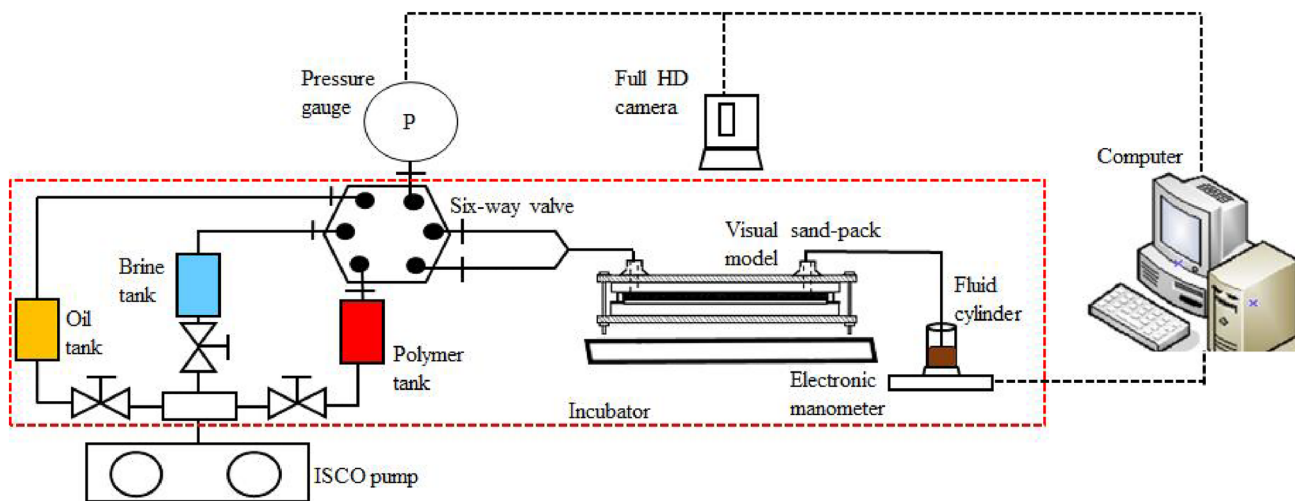


Fig. 2 The schematic diagram of experimental apparatus

power system used an ISCO pump to pump different fluids through the injection into the visual sand-packed model. The automatic dynamic monitoring system included a pressure gauge, electronic manometer, and full HD camera to transmit production performance data and oil/water distribution images to the computer during the displacement process.

The three fluids used in this experiment are oil, formation water, and polymer solution. The viscosity of the oil sample was 58 mPa s at 55 °C and the formation water salinity is 2.86×10^4 mg/L as shown in Table 1. The polymer solution with a concentration of 200 ppm has a viscosity of 70 mPa s at 55 °C. The glass beads were placed in water and polymer solution for the wettability test. After the test, the contact angle of porous media was not obviously affected by water and polymer solution. In particular, through the wettability test, the wettability of glass beads did not change evidently in this experiment.

Experimental scenario

WPA is an important technical method to adjust swept region during the development of reservoir. Considering the characteristics of well pattern setting in sand-packed model instead of considering the angle between the injection-production well line and the main line, three well pattern types are designed in this work as shown in Fig. 3.

Based on the visual sand-packed model with eight penetrating holes, three common well pattern types could be

used in the visual displacement experiment as shown in Fig. 4. The single injection well is arranged in the middle of one side in the four-spot well pattern and staggered well pattern. And then, the two production wells are arranged in the middle of the opposite and adjacent sides in the four-spot well pattern, respectively. In contrast, both production wells are arranged at opposite ends of the opposite side as shown in Fig. 4b. The production and injection wells of the five-point well pattern are arranged diagonally as shown in Fig. 4c.

The well pattern adjustment scheme was divided into two displacement phases, in which only the pattern type was adjusted. The fluid adjustment scenario is divided into three stages, which are primary water flooding (PWF), polymer flooding (PF), and subsequent water flooding (SWF). The design of the six experimental scenarios considers the influence of WPA and PF on SA as shown in Table 2. Scenarios I, II and III were designed to study the influence of WPA, and scenarios IV, V, and VI were designed to study the influence of injected fluid type adjustment.

In particular, although the well pattern type for scenario III was not changed, the placement of injection-production wells was changed. In the PF scenarios, the polymer solution was injected into the reservoir based on the original well pattern type during the subsequent flooding stage.

Table 1 The mineral composition of formation water

Type of ions	Na ⁺	Mg ²⁺	Ca ²⁺	CO ₃ ²⁻	HCO ₃ ⁻	Cl ⁻	SO ₄ ²⁻	Total
Concentration of ions (mg/L)	9121	152.2	320.2	2726.2	11606.4	4452.6	250.8	28629.4

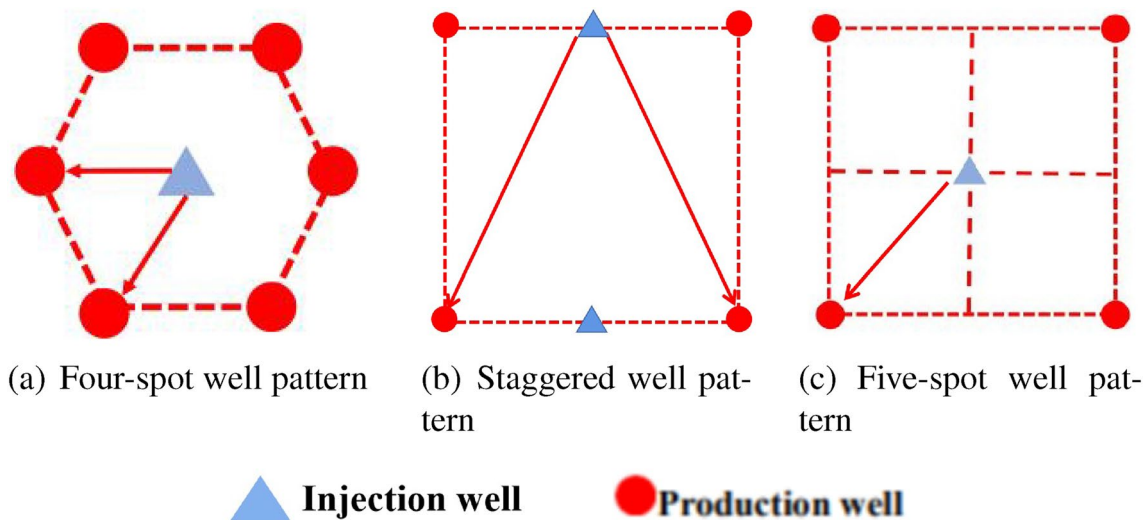


Fig. 3 The design diagram of three well patterns

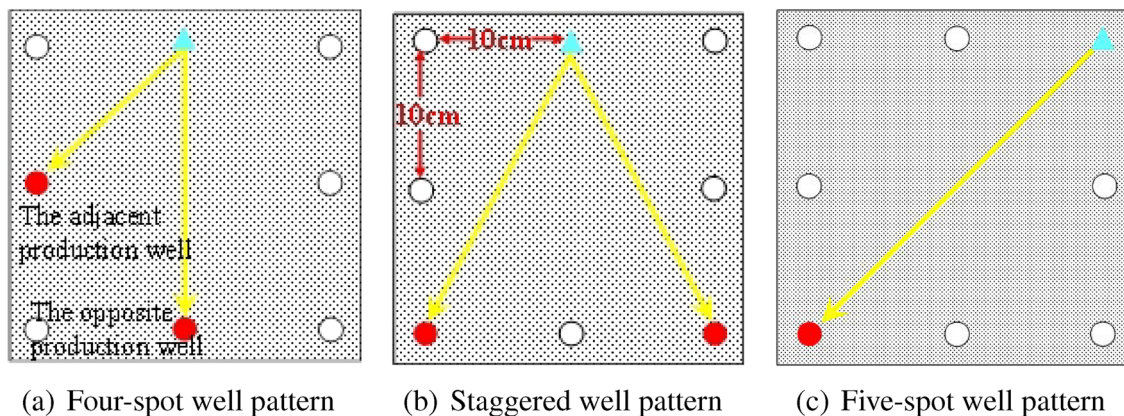


Fig. 4 The design diagram of three well patterns on the visual sand-packed model

Table 2 Visual sand-packed model of well pattern type and injection parameters

Scenario	Primary flooding stage		Subsequent flooding stage		Improvement measures
	Well pattern type	Fluid type	Well pattern type	Fluid type	
I	Four-spot	Water	Staggered	Water	WPA
II	Staggered	Water	Four-spot	Water	WPA
III	Five-spot	Water	Five-spot	Water	WPA
IV	Four-spot	Water	Four-spot	Polymer	PWF-PF-SWF
V	Staggered	Water	Staggered	Polymer	PWF-PF-SWF
VI	Five-spot	Water	Five-spot	Polymer	PWF-PF-SWF

Visualization procedure

After the completion of the experimental system connection and airtightness check, the specific experimental procedures and methods were as follows:

- (1) Oil reservoir model establishment procedure. After adjusting the internal temperature of the incubator to 55 °C, the visual sand-packed model was successively saturated with water and oil. Turn on the ISCO pump and select the injection speed of 0.5 mL/min. The model was considered to be fully saturated with water when the water flow at the outlet was stable (Wu et al. 2021). Then, in the same way, the reservoir model was saturated with oil at 55 °C. After the oil saturation process was completed, the data in the oil reservoir establishment procedure was analyzed and calculated. The residual water volume (V_{wi}) is divided by the pore volume (PV) to obtain the original water saturation (S_{wi}). The original oil volume (V_{oi}) and original oil

saturation (S_{oi}) were also obtained. The initial reserve abundance (SNA) could be calculated by Eq. 1:

$$SNA = V_{oi}/A_o \tag{1}$$

Where SNA is the reservoir abundance of oil; V_{oi} is the original oil volume and the size of the region with oil.

- (2) The primary flooding procedure. The water was injected into the sand-packed model at a constant flow rate of 0.5 mL/min. In the process, the pressure data at the injection well were obtained through the pressure gauge, and the production data were collected by the electronic manometer. Water cut data and stream-lined images in the primary flooding process were also collected. Until the water cut was close to 90%, the first displacement procedure tends to the end. In some regions that have been swept by the water, the abundance of residual reserve of the swept region after the displacement process should be calculated by formula Eq. 2:

$$SNA_r = (V_{oi} \cdot A_s/A_o - V_{co})/A_s \tag{2}$$

where SNA_r is the reservoir abundance of the remaining oil in the swept region after the displacement process; V_{or} is the volume that has been produced during the displacement process and is the size of the swept region. The SNA_{or} could quantitatively reflect the relative amount of remaining oil in the swept region after the displacement process, which was conducive to the comparison of development effects between different scenarios.

- (3) The subsequent flooding procedure. If the experimental scenario was to adjust the well pattern type, the amount and location of the injection well and production well needed to be adjusted to achieve the target well pattern type. And the total flow rate of injected fluid was still maintained at 0.5 mL/min. If the experimental scenario was to inject the polymer solution into the visual sand-packed model, inject a polymer into the model at 0.5 mL/min until a pre-determined amount was injected. And then, water was injected into the model until the water cut was closed to 90%. Different observation tasks need to be carried out in each experiment process as shown in Table 3.

Results and discussions

Intuitive performance of well pattern adjustment

The sand-packed model provided a mass of real-time pictures of streamlined pictures (Lyu et al. 2018). The distribution of oil and water phase in the model can be judged by the brightness of the images. Furthermore, the streamlines distribution under various experimental scenarios could be quantified by image analysis to calculate the oil saturation with the gray-scale method (Guo et al. 2017). On this basis, the formation reasons and improvement countermeasures of streamlines could be analyzed. Figure 5a, b, and c, respectively, show the streamlines distribution of scenarios I, II, and III after the primary flooding. The streamline in the four-point scenario has the shortest extended distance, while in the five-point scenario, the extended distance of streamlines is the farthest that other well pattern scenarios.

Figure 6 shows the streamlines distribution of the subsequent stage of the scenarios I, II, and III after the subsequent flooding. The position of the production well induces the streamline to extend further. The displacement images show the brownish-black of oil patches remain in the space between the streamlines. The streamlines are scattered in

Table 3 Observation tasks in different experimental procedures

Experimental procedure	Observation task
Oil reservoir establishment	(1) Macroscopic saturation alteration of oil and water (2) The front shape of oil during oil saturation
The primary flooding	(1) Macroscopic image of the streamlined trajectory (2) The size of the swept region
The subsequent flooding	(1) Macroscopic alteration of streamlined trajectory (2) Macroscopic shape alteration of the remaining oil region (3) The size of the swept region

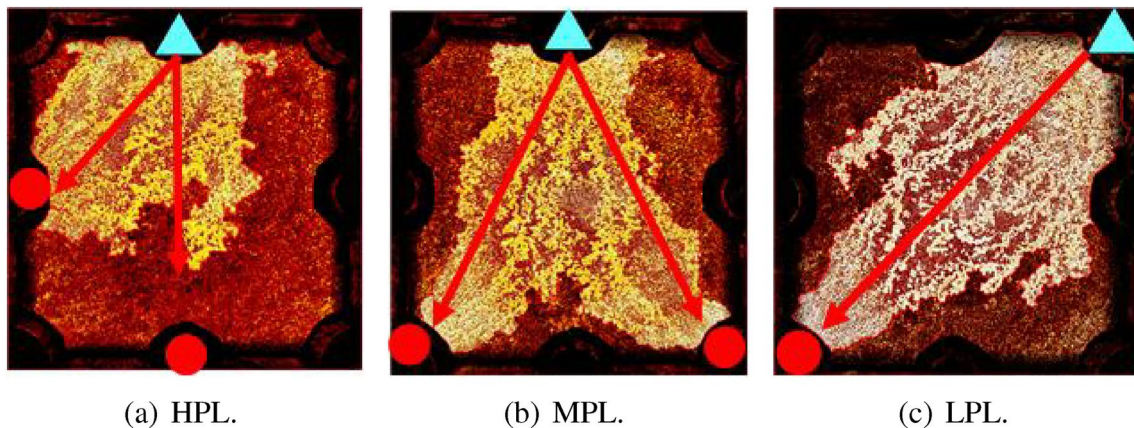


Fig. 5 Streamline images before WPA

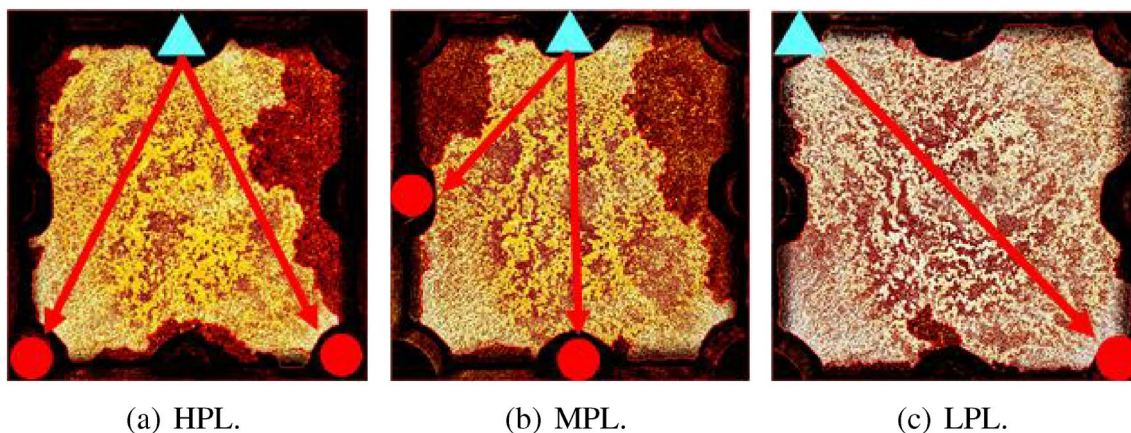


Fig. 6 Streamline images after WPA

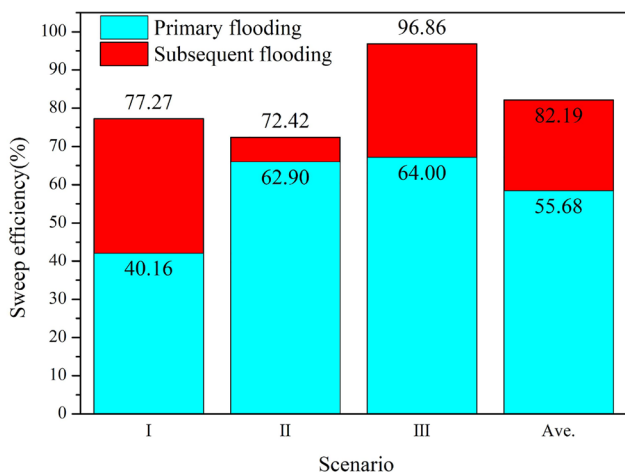


Fig. 7 The macroscopic sweep efficiency alteration by WPA

the middle of the visualization area, but the streamlines are dense in the area around the well as shown in Fig. 6a. However, the distribution of streamlines in the five-point well pattern is more dispersed and complicated as shown in Fig. 6c.

As shown in Fig. 7, based on the comparison between scenarios I and II when the four-point well pattern is transformed into a staggered well pattern, the sweep efficiency increases greatly, while the sweep efficiency did not increase significantly in the reverse well pattern sequence. In the initial flooding stage, scenario III has the best performance on the sweep efficiency than other scenarios.

Intuitive performance of polymer adjustment

The polymer solution can reduce the mobility of the displacing phase by increasing the viscosity of the displacing phase and by causing disproportionate permeability reduction (DPR) (Taber 1983). In addition, some researchers suggested that polymer had little influence on wettability

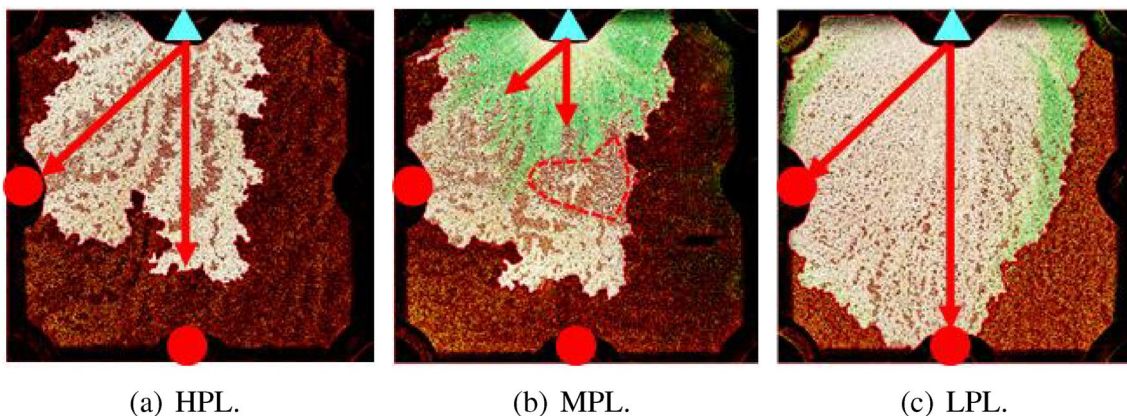


Fig. 8 Streamline images of PF for scenario IV

(Sharma et al. 2016; Li et al. 2020). The distribution and movement of polymers in porous media can be identified by the streamlines images.

The polymer with greenish fanned out from the injection well to the reservoir as shown in Fig. 8b. At the polymer front, there is brownish-black regions filled with remaining oil. During subsequent flooding, the greenish polymer was pushed to both sides of the swept region and the streamline extends from the adjacent well to the opposite well. Eventually, the streamlines formed a complete swept region between the injection well, adjacent production well and the opposite production well.

Similar to scenario IV, the brownish-black regions where there is plenty of remaining oil separates the fanned region with greenish polymer from the swept region generated during the PWF.

As shown in Fig. 10b, the brownish-black regions evidently distributed in the front of polymer slug. And subsequent water continuously pushed polymer into the reservoir.

Furthermore, the subsequent water along the injection-production well line further expanded the swept region.

At the above-mentioned form of streamlines, after the polymer entered the model to form a fan-shaped region centered on the injection well. In the fan-shaped region, a large number of black remaining oil spots were eliminated and the brightness was significantly increased, but the brightness of the polymer front was reduced as shown in the dotted line Figs. 8b, 9b, and 10b. The region of reduced brightness indicates increased internal oil saturation.

When subsequent water broke through the high polymer region, a large amount of polymer was pushed to the edge of the swept region as shown in Figs. 9c and 10c. When the subsequent water reentered the production well, the water cut quickly recovered to more than 90%.

By analyzing the results of the sweep efficiency as shown in Fig. 11, the effect of PF on macroscopic sweep efficiency is obvious. Under similar productive and geological conditions, scenario IV had the smallest increase in sweep

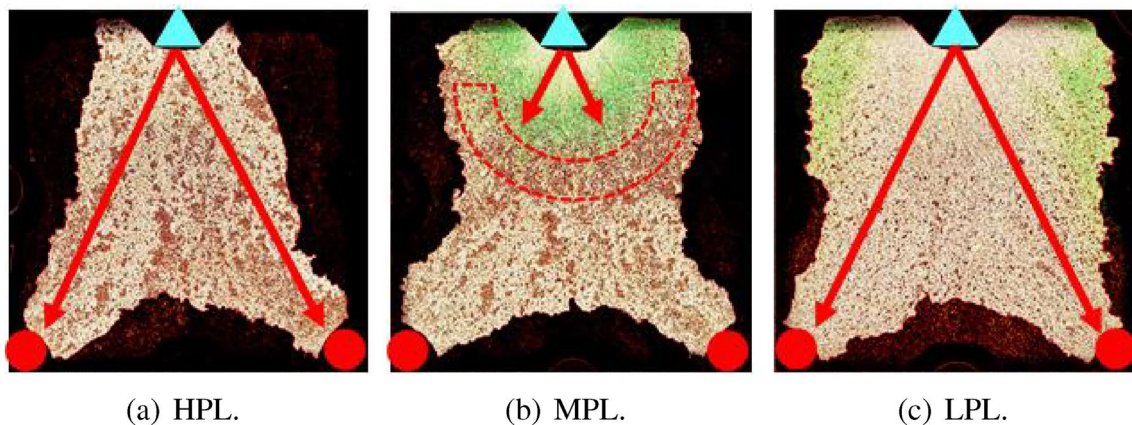


Fig. 9 Streamline images of PF for scenario IV

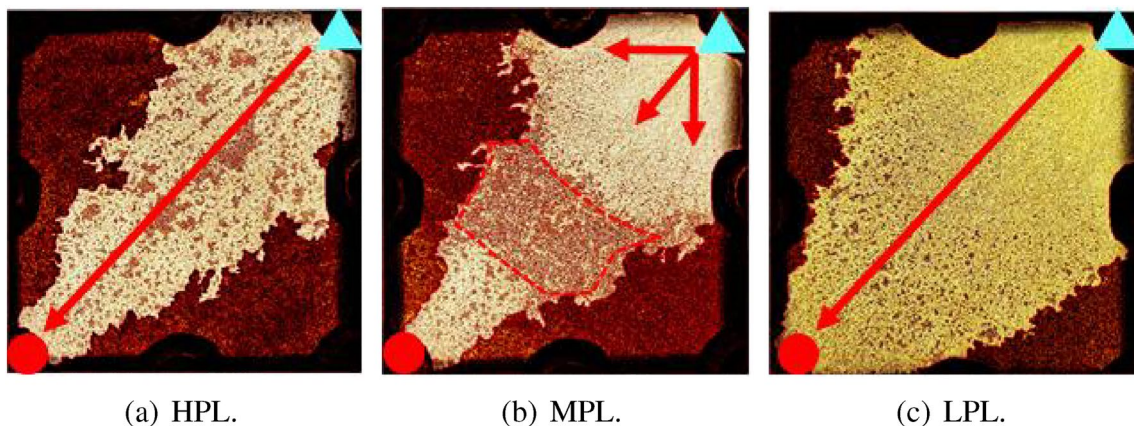


Fig. 10 Streamline images of PF for scenario VI

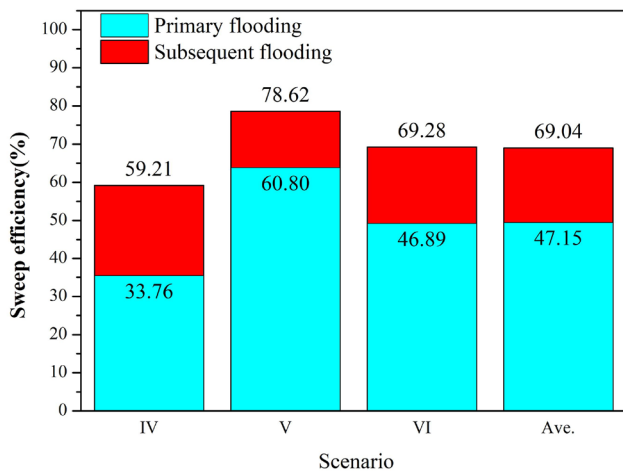


Fig. 11 The macroscopic sweep efficiency alteration by PF

efficiency, while scenario V increased. Interestingly, the sweep efficiency of scenario V remained the highest at different stages of the PF scenarios, while scenario IV still had the lowest sweep efficiency of all scenarios.

Analysis of swept region

Through the image binarization algorithm, the water channels generated by displacing fluid and black patches produced by viscous fingering were separated. The dark and bright pixels were counted by the grayscale algorithm (Onaka and Sato 2021; Wang et al. 2021). In addition, we acquire the migration rule of the position of the streamlines by comparing the brightness alteration in the swept region.

As the binarization images show, the streamlines distribution in the swept region varies greatly after PF as shown in Fig. 12. The polymer front advanced evenly and further

pushed the remaining oil toward the production well. There were obvious differences in the swept region formed after the fluid type was adjusted, which was caused by the viscosity difference between displacing fluid and displaced fluid. Because the viscosity of displacing fluid (water) is less than that of the displaced fluid (oil), the viscous fingering caused by the viscosity difference hurts the sweep efficiency. To display the influence of viscosity difference on the shape of swept region, the change rate of viscous fingering could be introduced to describe it in the 2D visual sand-packed model.

According to the statistics in the sand-packed model, most of the pore throat size was about 400 μm, which made the capillary force smaller than the viscous force, so the capillary force could be ignored when we established a mathematical model. Therefore, the influence of viscous force and gravity in Darcy flow was considered when we established the model. Meanwhile, polymer interfaces remain stable in the visualization region during PF because polymer molecules are difficult to diffuse efficiently into water at low shear rates. According to Darcy’s law, we can build a mathematical model of the front of polymer at the displacement interface based on the two dimensional model. The equation system is as follows (Saffman and Taylor 1958):

$$\begin{cases} dv_i/dr = 0 \\ v_i = d\Phi_r/dr + K_i A \rho_i g \sin \alpha / \mu_i \\ \Phi|_{r=r_{in}} = \Phi_{inj} \\ \Phi|_{r=r_{ro}} = \Phi_{pro} \end{cases} \quad (3)$$

where v_i denotes the fluid velocity at displacement interface; i denotes the type of fluid (aqueous phase or oil phase) and Φ_r denotes the velocity potential at the position of r . K_i and μ_i are the permeability and viscosity of the fluid in porous media. In addition, ρ_i denotes the density of the fluid and

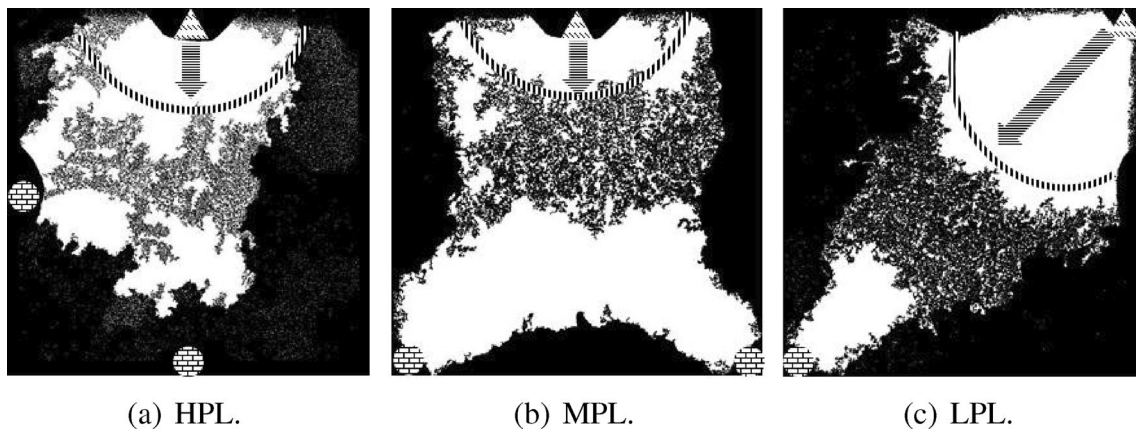


Fig. 12 Initial images of the multilayered heterogeneous reservoir

α denotes the horizontal angle of the model, which makes the mathematical model consider the influence of gravity on fluid percolating in porous media. The general solution of Eq. 3 is:

$$\Phi_i = (v_i - K_i A \rho_i g \sin \alpha / \mu_i) r + C \tag{4}$$

In the mathematical model, the distance between the injection well and displacement interface is assumed as r_f . The percolation region is divided into the oil phase percolation region and the aqueous phase percolation region with r_f as the boundary. The velocity potential of the injection well and displacement interface can be determined in the aqueous phase percolation region:

$$\begin{cases} \Phi_{inj} = (v_{in} - K_{in} A \rho_{in} g \sin \alpha / \mu_{in}) r_{inj} + C \\ \Phi_f = (v_{in} - K_{in} A \rho_{in} g \sin \alpha / \mu_{in}) r_f + C \end{cases} \tag{5}$$

The velocity potential of the displacement interface and the production well can be determined in the oil phase percolation region:

$$\begin{cases} \Phi_f = (v_{ed} - K_{ed} A \rho_{ed} g \sin \alpha / \mu_{ed}) r_f + C \\ \Phi_{pro} = (v_{ed} - K_{ed} A \rho_{ed} g \sin \alpha / \mu_{ed}) r_{pro} + C \end{cases} \tag{6}$$

where $v_i n$ denotes the velocity of displacing fluid; $v_e d$ denotes the velocity of displaced fluid and r denotes the distance between the injection well and production well. Equations 5 and 6 can be used to obtain the velocity potential of injection and production wells:

$$\begin{aligned} \Phi_{pro} - \Phi_{inj} + [K_{ed} \rho_{ed} (r_{pro} - r_f) / \mu_{ed} \\ + K_{in} \rho_{in} (r_f - r_{inj}) / \mu_{in}] A g \sin \alpha \\ = v_{in} (r_f - r_{inj}) + v_{ed} (r_{pro} - r_f) \end{aligned} \tag{7}$$

The stability of the displacement interface is often measured by the mobility ratio. When different phase velocities are affected by pressure, the pressure gradient is introduced to correlate the fluid velocity with the mobility ratio:

$$\begin{aligned} (\partial p / \partial n)_{in} / (\partial p / \partial n)_{ed} &= (v / \lambda)_{in} / (v / \lambda)_{ed} \\ &= (v_{in}) / (v_{ed}) \cdot (\mu_{in} K_{ed}) / (\mu_{ed} K_{in}) \end{aligned} \tag{8}$$

where p denotes the pressure of fluid; n denotes the distance in the normal direction and λ denotes the mobility. Equation 8 can be simplified by substituting the mobility ratio of displacing phase to the displaced phase (M_{in}):

$$v_{ed} = v_{in} \cdot (\mu_{ed} K_{in}) / (\mu_{in} K_{ed}) = v_{in} \cdot M_{in} \tag{9}$$

The velocity of displacing fluid v_{in} can be obtained by substituting Eq. 9 into Eq. 7:

$$\begin{aligned} v_{in} = - \frac{\Phi_{inj} - \Phi_{pro}}{(1 - M_{in}) r_f + M_{in} (r_{pro} - r_{inj})} \\ \left[1 - \frac{K_{ed} \rho_{ed} (r_{pro} - r_f) / \mu_{in} + K_{in} \rho_{in} (r_f - r_{inj}) / \mu_{in}}{\Phi_{inj} - \Phi_{pro}} A g \sin \alpha \right] \end{aligned} \tag{10}$$

The sand-packed model is placed on the horizontal table, which makes the value $\sin \alpha$ equal to 0. The above work makes it convenient to calculate the true percolating velocity on the displacement interface.

$$u_{in} (r_f) = \frac{v_{in}}{\phi} = \frac{\Phi_{pro} - \Phi_{inj}}{\phi [(1 - M_{in}) r_f + M_{in} (r_{pro} - r_{inj})]} \tag{11}$$

where u_{in} denotes the true percolation velocity of the displacing fluid. Since viscous fingering occurs when two kinds of fluids with viscosity differences in the flow of porous media, the distance of influence at the displacement interface can be expressed as ε :

$$\begin{aligned} \frac{d\varepsilon}{d\tau} &= u_{in} (r_f + \varepsilon) - u_{in} (r_f) \\ &= \frac{\Phi_{pro} - \Phi_{inj}}{\phi} \left[\frac{1}{(1 - M_{in}) (r_f + \varepsilon) + M_{in} r_{pro} - r_{inj}} \right. \\ &\quad \left. - \frac{1}{(1 - M_{in}) r_f + M_{in} r_{pro} - r_{inj}} \right] \\ &\approx \frac{(\Phi_{inj} - \Phi_{pro}) (M_{in} - 1) \varepsilon}{\phi [(1 - M_{in}) r_f + M_{in} r_{pro} - r_{inj}]^2} \end{aligned} \tag{12}$$

The change rate of viscous fingering (σ) is introduced to characterize the mutation degree of displacement interface:

$$\begin{aligned} \sigma = \frac{1}{\varepsilon} \frac{d\varepsilon}{d\tau} &= \frac{(\Phi_{inj} - \Phi_{pro}) (M_{in} - 1)}{\phi [(1 - M_{in}) r_f + M_{in} r_{pro} - r_{inj}]^2} \\ &= C_p (M_{in} - 1) \quad (C_p > 0) \end{aligned} \tag{13}$$

According to Eq. 13, it is clear that the rate of VF depends on the value of the mobility ratio when other factors have little influence on viscous fingering. Furthermore, the

Table 4 The relationship between viscous fingering (VF) and mobility ratio

Mobility ratio	Change rate of VF	Displacement front shape	Strength of VF
$M_1 > 1$	$\sigma > 0$	Sharp and branching shape	Increased
$M_1 = 1$	$\sigma = 0$	Stable and unchanged shape	Constant
$M_1 < 1$	$\sigma < 0$	Gentle and fan shape	Decreased

relationship between viscous fingering and mobility ratio is determined as shown in Table 4.

When the polymer was injected into the sand-packed model at low speed, it is difficult for the polymer to diffuse from the polymer solution into the water environment created by the primary flooding to improve the viscosity of the water, which makes the polymer solution and water considered as two type of fluids with viscosity difference. Therefore, the polymer solution pushed the water and the remaining oil to percolate into the swept region at the displacement interface during the PF. The mobility ratio between the polymer solution and water during PF is approximately 0.0125 at 55 °C and the mobility ratio between the polymer solution and remaining oil during PF is approximately 0.6875. Because the water generated by primary flooding is easy to flow along the water channels, the oil saturation in front of the polymer interface is increasing, and the remaining oil tends to push the water (Pinilla et al. 2021).

Numerical analysis of production performance

The production dynamic curves that includes oil recovery, water cut, and pressure are shown in Fig. 13. Based on the analysis of the production performance curve, the breakthrough time and pressure peak for each well pattern type could be compared in the development process. Oil recovery from primary and subsequent water flooding in different scenarios can also reflect the influence of these SA methods on oil improvement as shown in Table 5.

The production performance data during the primary flooding could only reflect the development effect under different well pattern types. The breakthrough time (PV) was an important parameter reflecting the characteristics of early streamline development. The breakthrough time of scenario I was earlier than that of scenario II, and the breakthrough time of scenario II was also earlier than that of scenario III. Similarly, the pressure peak of scenario I was smaller than that of scenario II and scenario III. According to Fig. 5, the distance between the injection well and production well was 141.4 mm in scenario I, 232.2 mm in scenario II, and 282.8 mm in scenario III (the ratio was $\sqrt{2} : \sqrt{5} : 2\sqrt{2}$), which was similar to the ratio of breakthrough time in the three scenarios.

Figure 14 shows a comparison of oil recovery for all scenarios at primary and subsequent stages. By comparing the oil recovery of different scenarios, it was found that the five-spot well pattern had the highest oil recovery and the four-spot well pattern had the lowest oil recovery during primary flooding, but the oil recovery values of the three well patterns were similar.

According to Figs. 7, 11, and 14, the average increase in sweep efficiency was 47.59% by WPA and 46.42% by PF. Average oil recovery was improved by 57.71% of WPA and

110.82% of PF. By comparing the sweep efficiency with oil recovery, we found that the increase in oil recovery was much greater than the increase in the macroscopic sweep efficiency in the PF scenarios, which did not occur in the WPA scenarios. Next, we need to explore the reasons for this phenomenon.

Macro and micro-analysis of SA

By measuring the area of the swept region and the volume of oil produced, SNA_r , each scenario could be calculated according to Eq. 2, which could quantitatively reflect the amount of remaining oil in the swept region in different scenarios as shown in Table 5.

Then SNA_r after subsequent flooding was reduced in the PF scenarios, which indicated a significant reduction in the amount of remaining oil in the swept region. In the WPA scenarios, the SNA_r did not reduce the amount of remaining oil in the swept region produced by primary flooding. To study the cause of an apparent decline in the amount of remaining oil in the swept region, we must get down to the microscale to understand what is happening.

Microscopic observation method is used to observe the remaining oil occurrence state in the water channels (Urbissinova and Kuru 2010; Alizadeh et al. 2014). The distribution of oil and water in scenario III at different observation scales is shown in Fig. 15a, b, and c. And the distribution of oil, water, and polymer in the scenario IV at different observation scales can be observed in Fig. 15d, e, and f.

As shown in Fig. 15b, there were a large number of flake remaining oil in the swept region at the microscopic scale. Around the flake remaining oil, water could flow easily along the water channels with low resistance as shown in Fig. 15c. After the well pattern type was adjusted, the subsequent water flowed along the new streamlines. However, when the new streamlines passed through the original water channels generated by primary flooding, the subsequent water flowed along the original water channels, so that the remaining oil around the original water channels was not affected obviously.

To develop the unswept region with flake remaining oil, it is necessary to improve the resistance in the water channels around the flake remaining oil, forcing the subsequent fluid into the region where flake remaining oil was located. The WPA scenario is difficult to realize the development of flake remaining oil around water channels.

As the polymer entered the sand-packed model, the brightness increased in the polymer fan-shaped region as shown in Fig. 15d. As the polymer preferentially entered the water channel with low resistance, part of the residual polymer accumulated in the nodes of the water channels as shown in Fig. 15e. As the polymer entered the sand-packed model, the resistance in the water channels was

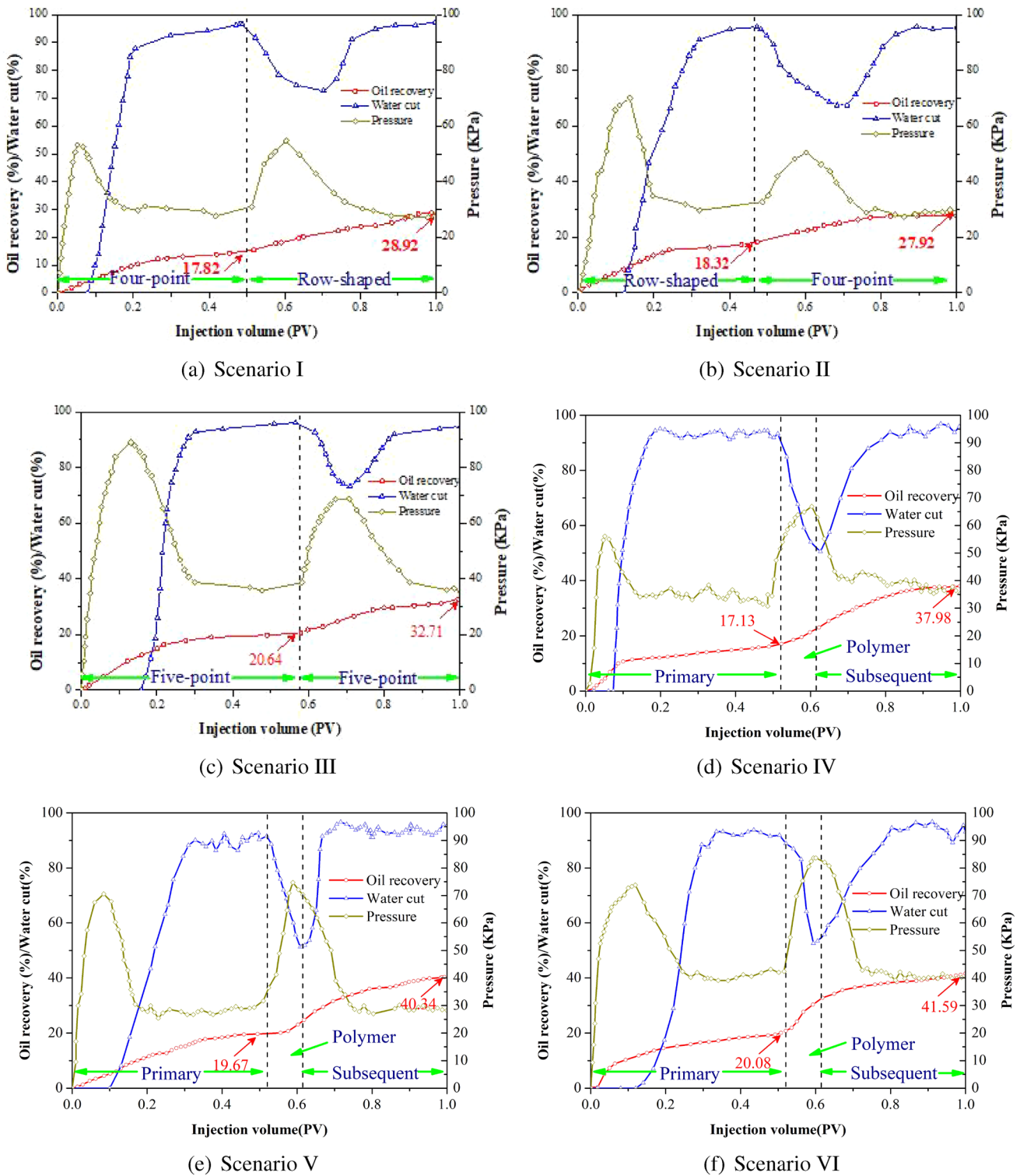


Fig. 13 Oil recovery, water cut, and pressure versus injected volume in different scenarios

gradually increased by residual polymer, which changed the flow direction of the subsequent water. The strength of VF is weakened in the microscopic images because with the polymer in the water channel, the resistance gap at

the waterfront was drawn in. As shown in Fig. 15f, some remaining oil that is difficult to be exploited still existed in the corner or throats and may need to be developed in other ways.

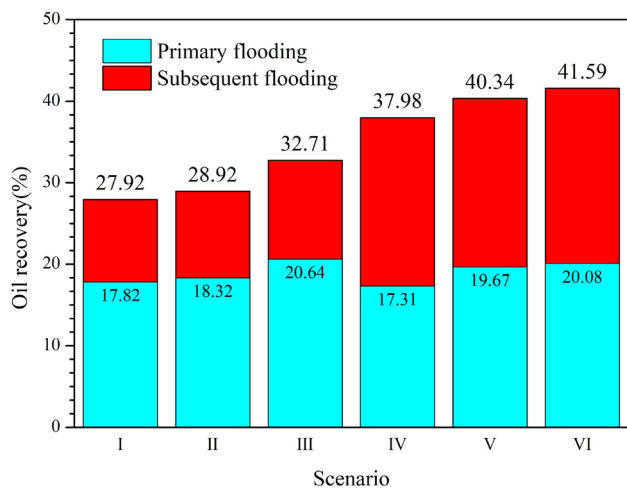


Fig. 14 Oil recovery at different stages in different scenarios

By comparing the microscopic images of different scenarios, we can understand the strength of the VF phenomenon. Moreover, we can find remaining oil on the rock surface or narrow throat after PF. These remaining oil needs to be effectively displaced by surfactant-polymer or other

Table 5 Visual sand-packed model of well pattern type and injection parameters

Scenario	Breakthrough time(PV)	Pressure peak (Kpa)	SNA_r	
			PWF	SWF
I	0.078	53.7	0.025	0.027
II	0.122	70.0	0.032	0.031
III	0.158	89.1	0.028	0.030
IV	0.078	66.9	0.023	0.016
V	0.121	74.7	0.031	0.022
VI	0.154	83.7	0.026	0.018

chemical methods (Shen et al. 2009; Shandrygin et al. 2016), which is worth further study and exploration.

Conclusions

Through experimental and mathematical analysis, the streamline adjustment (SA) after well pattern adjustment (WPA) or polymer flooding (PF) can be visually reflected. The improvement rules of the two methods on SA were

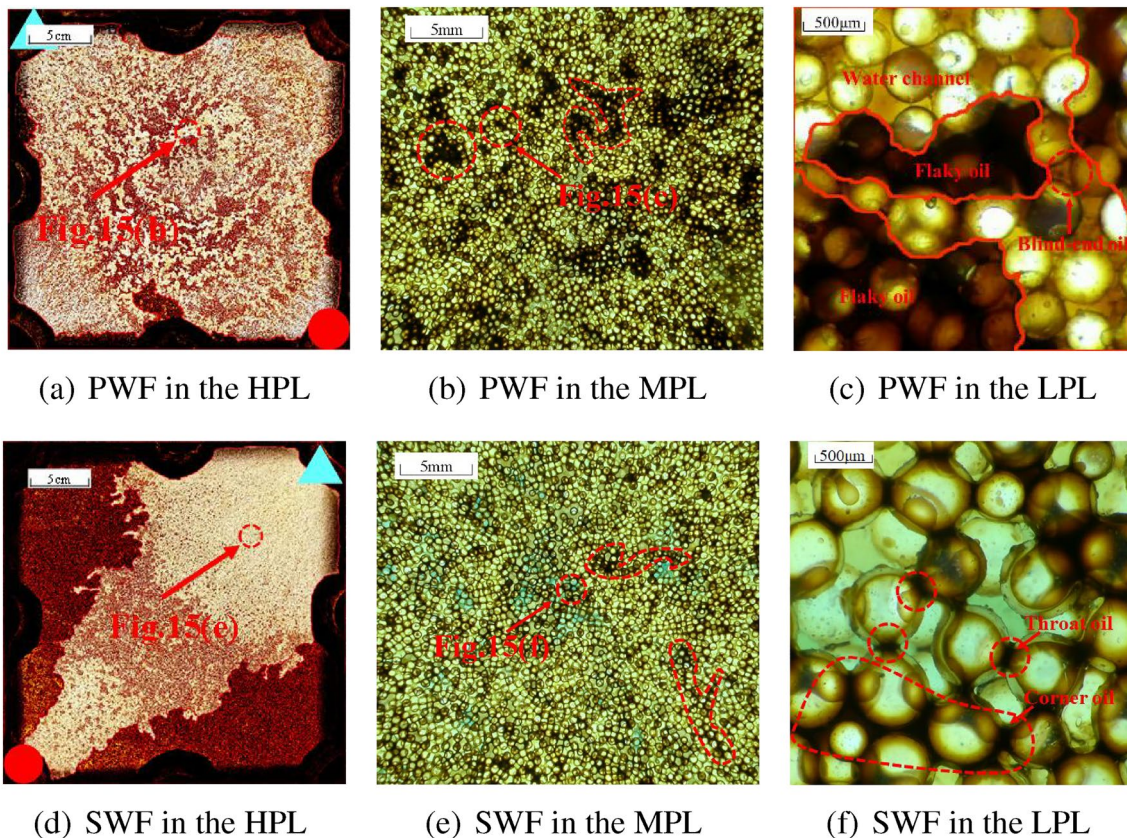


Fig. 15 Oil recovery, water cut, and pressure versus injected volume in different scenarios

revealed from macro and micro scales. The following conclusions can be made:

- The pressure in the reservoir is redistributed as a result of the WPA so that the water channel generated by primary water flooding is no longer the pressure relief channel. Streamline density and coverage area are important factors for SA.
- After PF, the front of the high viscosity polymer spread out in a fan-shape on a macroscopic scale to weaken the strength of viscous fingering (VF). The PF can improve sweep efficiency by blocking the water channels and promote fluid into the unswept region by increasing displaced pressure.
- The strength of VF could also affect the development of streamlines. When the mobility ratio is large, the VF strength is high, which causes the streamlines to diverge between the injection well and the production well. When the mobility ratio is small, the influence of VF is weak, which makes the streamlines advance evenly fan-shaped.
- In the two technologies of SA, profile control and water plugging is the key to enhancing oil recovery. Through the 2D displacement images, it is clear that the WPA can expand the swept region of the streamlines, while PF denser the streamlines. The WPA uses the remaining oil outside the swept region by produce new streamlines.

Acknowledgments We declare that we do not have any commercial or associative interest that represents a conflict of interest in connection with the work submitted. The research work is supported by the National Natural Science Foundation of China (No. U20B6003) and the Science Foundation of China University of Petroleum, Beijing (No. 2462020YXZZ032).

Funding This study was funded by the National Natural Science Foundation of China Joint Fund Project (No.U20B6003) and Science Foundation of China University of Petroleum, Beijing (No.2462022BJRC003) for finical support.

Open Access This article is licensed under a Creative Commons Attribution 4.0 International License, which permits use, sharing, adaptation, distribution and reproduction in any medium or format, as long as you give appropriate credit to the original author(s) and the source, provide a link to the Creative Commons licence, and indicate if changes were made. The images or other third party material in this article are included in the article's Creative Commons licence, unless indicated otherwise in a credit line to the material. If material is not included in the article's Creative Commons licence and your intended use is not permitted by statutory regulation or exceeds the permitted use, you will need to obtain permission directly from the copyright holder. To view a copy of this licence, visit <http://creativecommons.org/licenses/by/4.0/>.

References

- Al-Shalabi EW, Ghosh B (2016) Effect of pore-scale heterogeneity and capillary-viscous fingering on commingled waterflood oil recovery in stratified porous media. *J Pet Eng*. <https://doi.org/10.1155/2016/1708929>
- Alizadeh A, Khishvand M, Ioannidis M (2014) Multi-scale experimental study of carbonated water injection: an effective process for mobilization and recovery of trapped oil. *Fuel* 132:219–235. <https://doi.org/10.1016/j.fuel.2014.04.080>
- Behzadi SH, Towler BF (2009) A new eor method. In: SPE annual technical conference and exhibition, onepetro. <https://doi.org/10.2118/123866-MS>
- Cheraghian G (2015) An experimental study of surfactant polymer for enhanced heavy oil recovery using a glass micromodel by adding nanoclay. *Pet Sci Technol* 33:1410–1417. <https://doi.org/10.1080/10916466.2015.1062780>
- Christensen JR, Stenby EH, Skauge A (2001) Review of wag field experience. *SPE Reserv Eval Eng* 4:97–106. <https://doi.org/10.2118/71203-PA>
- Cottin C, Bodiguel H, Colin A (2010) Drainage in two-dimensional porous media: from capillary fingering to viscous flow. *Phys Rev E* 82:046315. <https://doi.org/10.1103/PhysRevE.82.046315>
- Du QJ, Pan GM, Hou J (2019) Study of the mechanisms of streamline-adjustment-assisted heterogeneous combination flooding for enhanced oil recovery for post-polymer-flooded reservoirs. *Pet Sci* 16:606–618. <https://doi.org/10.1007/s12182-019-0311-0>
- Grinestaff G (1999) Waterflood pattern allocations: quantifying the injector to producer relationship with streamline simulation. In: SPE western regional meeting, onepetro. <https://doi.org/10.2118/54616-MS>
- Guo F, Aryana SA (2018) Improved sweep efficiency due to foam flooding in a heterogeneous microfluidic device. *J Petrol Sci Eng* 164:155–163. <https://doi.org/10.1016/j.petrol.2018.01.042>
- Guo Y, Liang Y, Cao M (2017) Flow behavior and viscous-oil-micro-displacement characteristics of hydrophobically modified partially hydrolyzed polyacrylamide in a repeatable quantitative visualization micromodel. *SPE J* 22:1448–1466. <https://doi.org/10.2118/185185-PA>
- Imqam A, Wang Z, Bai B (2017) Preformed-particle-gel transport through heterogeneous void-space conduits. *SPE J* 22:1437–1447. <https://doi.org/10.2118/179705-PA>
- Jackson S, Power H, Giddings D (2017) The stability of immiscible viscous fingering in hele-shaw cells with spatially varying permeability. *Comput Methods Appl Mech Eng* 320:606–632. <https://doi.org/10.1016/j.cma.2017.03.030>
- Jian H, Zhang SK, Du QJ (2008) A streamline-based predictive model for enhanced-oil-recovery potentiality. *J Hydrodyn Ser B* 20:314–322. [https://doi.org/10.1016/S1001-6058\(08\)60063-3](https://doi.org/10.1016/S1001-6058(08)60063-3)
- Li Z, Ayirala S, Mariath R (2020) Microscale effects of polymer on wettability alteration in carbonates. *SPE J* 25:1884–1894. <https://doi.org/10.2118/200251-PA>
- Liu F, Wu X, Zhou W (2020) Application of well pattern adjustment for offshore polymer flooding oilfield: a macro-scale and micro-scale study. *Chem Technol Fuels Oils* 56:441–452. <https://doi.org/10.1007/s10553-020-01155-1>
- Lu C, Liu H, Zhao W (2017) Visualized study of displacement mechanisms by injecting viscosity reducer and non-condensable gas to assist steam injection. *J Energy Inst* 90:73–81. <https://doi.org/10.1016/j.joei.2015.10.005>
- Lyu X, Liu H, Pang Z, Sun Z (2018) Visualized study of thermochemistry assisted steam flooding to improve oil recovery in heavy oil reservoir with glass micromodels. *Fuel* 218:118–126. <https://doi.org/10.1016/j.fuel.2018.01.007>

- Mack J, Smith J (1994) In-depth colloidal dispersion gels improve oil recovery efficiency. In: SPE/DOE improved oil recovery symposium, OnePetro. <https://doi.org/10.2118/27780-MS>
- Onaka Y, Sato K (2021) Dynamics of pore-throat plugging and snow-ball effect by asphaltene deposition in porous media micromodels. *J Petrol Sci Eng* 207:109176. <https://doi.org/10.1016/j.petrol.2021.109176>
- Pei H, Zhang G, Ge J (2012) Comparative effectiveness of alkaline flooding and alkaline-surfactant flooding for improved heavy-oil recovery. *Energy Fuels* 26:2911–2919. <https://doi.org/10.1021/ef300206u>
- Pinilla A, Asuaje M, Ratkovich N (2021) Experimental and computational advances on the study of viscous fingering: an umbrella review. *Heliyon* 7:e07614. <https://doi.org/10.1016/j.heliyon.2021.e07614>
- Pratama RA, Babadagli T (2021) New formulation of tertiary amines for thermally stable and cost-effective chemical additive: synthesis procedure and displacement tests for high-temperature tertiary recovery in steam applications. *SPE J* 26:1572–1589. <https://doi.org/10.2118/201769-PA>
- Saffman PG, Taylor GI (1958) The penetration of a fluid into a porous medium or hele-shaw cell containing a more viscous liquid. *Proc R Soc Lond A* 245:312–329. <https://doi.org/10.1098/rspa.1958.0085>
- Samier P, Quettier L, Thiele M (2001) Applications of streamline simulations to reservoir studies. In: SPE reservoir simulation symposium, onepetro. <https://doi.org/10.2118/66362-MS>
- Sandiford B (1964) Laboratory and field studies of water floods using polymer solutions to increase oil recoveries. *J Pet Technol* 16:917–922. <https://doi.org/10.2118/844-PA>
- Shams M, Currie I, James D (2003) The flow field near the edge of a model porous medium. *Exp Fluids* 35:193–198. <https://doi.org/10.1007/s00348-003-0657-2>
- Shandrygin A, Shelepov V, Ramazanov R (2016) Mechanism of oil displacement during polymer flooding in porous media with micro-inhomogeneities. In: SPE russian petroleum technology conference and exhibition, onepetro. <https://doi.org/10.2118/182037-MS>
- Sharma T, Iglauer S, Sangwai JS (2016) Silica nanofluids in an oil-field polymer polyacrylamide: interfacial properties, wettability alteration, and applications for chemical enhanced oil recovery. *Ind Eng Chem Res* 55:12387–12397. <https://doi.org/10.1021/acs.iecr.6b03299>
- Shen P, Wang J, Yuan S (2009) Study of enhanced-oil-recovery mechanism of alkali/surfactant/polymer flooding in porous media from experiments. *SPE J* 14:237–244. <https://doi.org/10.2118/126128-PA>
- Taber JJ (1983) Technical screening guides for the enhanced recovery of oil. In: SPE annual technical conference and exhibition, OnePetro. <https://doi.org/10.2118/12069-MS>
- Tongwa P, Bai B (2016) Mitigating permeability contrasts in heterogeneous reservoirs using advanced preformed particle gels. *Int J Oil Gas Coal Technol* 13:103–118. <https://doi.org/10.2118/27780-MS>
- Urbissinova TS, Kuru E (2010) Effect of elasticity during viscoelastic polymer flooding: a possible mechanism of increasing the sweep efficiency. *J Can Pet Technol* 49:49–56. <https://doi.org/10.2118/133471-PA>
- Van SL, Chon BH (2016) Well-pattern investigation and selection by surfactant-polymer flooding performance in heterogeneous reservoir consisting of interbedded low-permeability layer. *Korean J Chem Eng* 33:3456–3464. <https://doi.org/10.1007/s11814-016-0190-7>
- Wang D, Cheng J, Yang Q (2000) Viscous-elastic polymer can increase microscale displacement efficiency in cores. In: SPE annual technical conference and exhibition, OnePetro. <https://doi.org/10.2118/63227-MS>
- Wang H, Hou J, Guo Z (2020a) Evaluation of different well converting patterns with the distribution of streamlines on ultra high water cut reservoir. In: offshore technology conference Asia, OnePetro. <https://doi.org/10.4043/30329-MS>
- Wang Y, Liu H, Guo M (2021) Image recognition model based on deep learning for remaining oil recognition from visualization experiment. *Fuel* 291:120216. <https://doi.org/10.1016/j.fuel.2021.120216>
- Wang Y, Liu H, Zhang Q (2020) Pore-scale experimental study on eor mechanisms of combining thermal and chemical flooding in heavy oil reservoirs. *J Petrol Sci Eng* 185:106649. <https://doi.org/10.1016/j.petrol.2019.106649>
- Wang Y, Zhao F, Bai B (2010) Optimized surfactant ift and polymer viscosity for surfactant-polymer flooding in heterogeneous formations. In: SPE improved oil recovery symposium, OnePetro. <https://doi.org/10.2118/127391-MS>
- Wei B, Romero-Zerón L, Rodrigue D (2014) Oil displacement mechanisms of viscoelastic polymers in enhanced oil recovery (eor): a review. *J Pet Explor Prod Technol* 4:113–121. <https://doi.org/10.1007/s13202-013-0087-5>
- Wu Z, Huiqing L, Cao P (2021) Experimental investigation on improved vertical sweep efficiency by steam-air injection for heavy oil reservoirs. *Fuel* 285:119138. <https://doi.org/10.1016/j.fuel.2020.119138>
- Wu Z, Liu H, Pang Z (2016) Pore-scale experiment on blocking characteristics and eor mechanisms of nitrogen foam for heavy oil: a 2d visualized study. *Energy Fuels* 30:9106–9113. <https://doi.org/10.1021/acs.energyfuels.6b01769>
- Yuan XC, Yang FB (2003) Regrouping adjusting of the producer-injector well-pattern in the high aquifer period of oilfield development. *Pet Explor Dev* 30:94–96
- Zhao P, He S, Cai M (2020) Streamline simulation based vector flow field characterization and reconstruction method for high water cut reservoir. In: international petroleum technology conference, onepetro. <https://doi.org/10.2523/IPTC-20291-Abstract>
- Zheng J, Wang Z, Ju Y (2021) Visualization of water channeling and displacement diversion by polymer gel treatment in 3d printed heterogeneous porous media. *J Pet Sci Eng* 198:108238. [https://doi.org/10.1016/S1876-3804\(18\)30033-8](https://doi.org/10.1016/S1876-3804(18)30033-8)
- Zhiwang Y, Baoquan Y, Li Y (2018) Water-cut rising mechanism and optimized water injection technology for deepwater turbidite sandstone oilfield: A case study of akpo oilfield in niger delta basin, west africa. *Pet Explor Dev* 45:302–311. [https://doi.org/10.1016/S1876-3804\(18\)30033-8](https://doi.org/10.1016/S1876-3804(18)30033-8)
- Zolfaghari R, Abdullah LC, Biak DR (2018) Cationic surfactants for demulsification of produced water from alkaline-surfactant-polymer flooding. *Energy Fuels* 33:115–126. <https://doi.org/10.1021/acs.energyfuels.8b03266>

Publisher's Note Springer Nature remains neutral with regard to jurisdictional claims in published maps and institutional affiliations.